Nuclear Inst. and Methods in Physics Research, A 1020 (2021) 165888

Contents lists available at ScienceDirect

Nuclear Inst. and Methods in Physics Research, A

journal homepage: www.elsevier.com/locate/nima

Optical transition radiation screens: A numerical procedure to choose the most performing material

F. Cioeta [a,*], D. Alesini [a], M. Ciambrella [c], D. Cortis [b], V. Lollo [a], M. Marongiu [b], A. Mostacci [c], L. Palumbo [c], V. Pettinacci [b], A. Variola [a]

[a] National Institute for Nuclear Physics (INFN), National Laboratory of Frascati, 00044 Frascati, Italy
[b] National Institute for Nuclear Physics (INFN), Section of Rome, 00185 Rome, Italy
[c] Department of Basic and Applied Sciences for Engineering, Sapienza University of Rome, 00185 Rome, Italy

ARTICLE INFO

Keywords:
Matter-radiation interaction
Gamma beam source
Optical transition radiation screen
Finite element analysis
ANSYS® APDL

ABSTRACT

In the field of diagnostics applied to particle accelerators, and more specifically when it comes to linear electron accelerators, OTR screens represent one of the most widespread and used techniques for beam monitoring. These devices must be able to withstand the thermal stress that the several bunches induce by hitting the surface at high frequency, without compromising the optical performance following the possible induced deformations. This paper presents a complete methodology to predict the behaviour of the OTR screens – thermal, mechanical and optical – for a given beam and screen material with the aim to define guidelines for the optimal target material selection.

Contents

1. Introduction

A new Gamma Beam System (GBS) based on a high brightness electron beam linear accelerator (LINAC) has been designed for the "Extreme Light Infrastructure – Nuclear Physics" (ELI-NP) project. The machine is an advanced source of gamma rays up to ≈ 20 MeV based on Compton back scattering effect, thanks to which electrons can reach a maximum kinetic energy of ≈ 740 MeV [1]. The nominal electron beam in the GBS machine consists of trains of 32 electron bunches of 250 pC each, separated by 16 ns, distributed along a 512 ns RF pulse, with a repetition rate of 100 Hz. The GBS design relies on Optical Transition Radiation (OTR) screens to evaluate the transverse beam profile and a wide range of other beam parameters in operation. This kind of device has been widely used in high-energy facilities such as SPARC Lab, DESY or CTF3 among others [2–4]. The design choice is justified by several advantages that OTR screens provide for beam diagnostics: the instantaneous emission process allowing fast single shot measurements, the good linearity (when coherent effects can be neglected) and the possibility to make additional measurements of the beam energy by means of the observation of its angular distribution [5]. Moreover, it leads to the possibility to measure the beam energy and the divergence by means of angular distribution observations [6]. The beam profile monitor used in the GBS machine is shown in Fig. 1. The OTR screen has an inclination of 45° with respect to the beam axis and the image observation is performed at 90°. The beam image is reflected using standard optic instruments and the intensity of the recorded beam footprint gives the measure of the particle beam spot [7].

* Corresponding author.
E-mail address: fara.cioeta@lnf.infn.it (F. Cioeta).

https://doi.org/10.1016/j.nima.2021.165888
Received 22 October 2019; Received in revised form 27 September 2021; Accepted 6 October 2021
Available online 16 October 2021

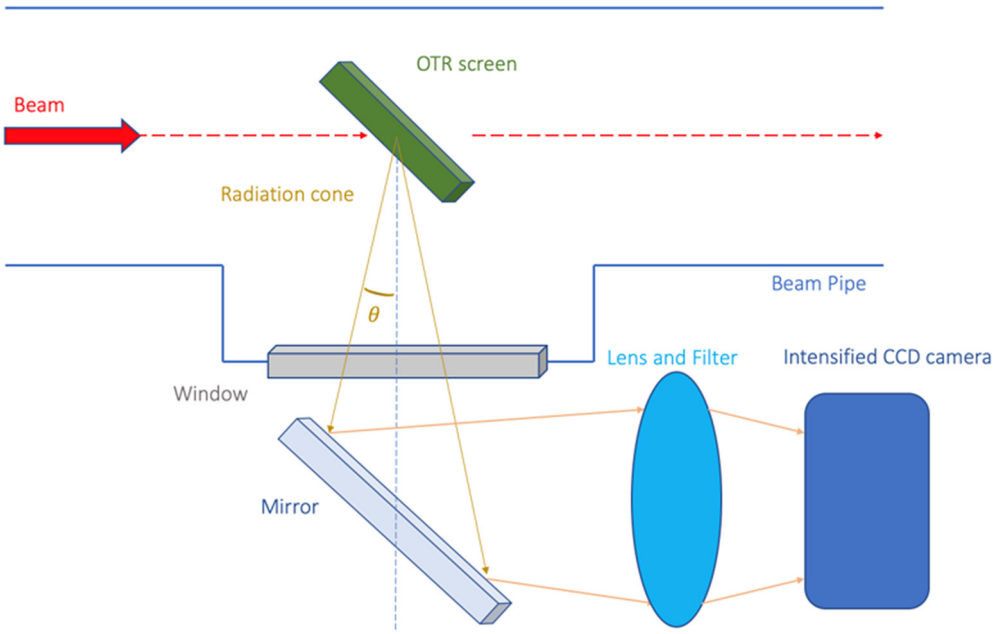

Fig. 1. Conceptual layout of the spot size diagnostics based on OTR screen for the GBS machine. The distance between the OTR screen and the optic lenses is 40 cm, while the distance between the optic lenses and the camera is 20 cm [8].

The beam diagnostics in OTR systems relies on the photon radiation that is emitted when its charged particles cross the boundary between the vacuum and the screen material, i.e. two media with different optical properties such as the different dielectric constant [9]. Appropriate surface flatness and high reflectivity of the OTR screen positively influence the photon emissions and, consequently, they are fundamental to reach a high resolution of the diagnostics system. These qualities must be preserved during the whole accelerator operation, especially in high-charge applications as for the GBS machine. On the other hand, the charged particles of the beam deposit considerable amounts of energy in the OTR screen material due to the interactions with its atoms. This phenomenon produces an increase of local temperature that is generally quite below the melting point. However, the temperature gradient produces deformations on the OTR screen surface that may influence the quality of the beam footprint image. For instance, Ross et al. [10] prove that a high charge beam, as in the case of the GBS machine, could damage the OTR screen, compromising the spot size measurements.

For this reason, it is recommended to study the effect of heat-induced target deformations on OTR measurements. Furthermore, although the maximum stresses are generally below the elastic limit, the pulsed nature of the beam determines the reproduction of thermal cycles and associated deformation-stress cycles that may determine the fatigue failure of the OTR screen. For example, OTR screens made of Silicon with an Aluminium coating are commonly used in high quality diagnostics in high brightness linear accelerator, i.e. the SPARC injector operating at National Laboratory of Frascati (LNF) [11]. However, the SPARC-like screens could not sustain the stress caused by the GBS beam according to previous studies [9,12]. Therefore, GBS is going to use monocrystalline Silicon screens which represent a good compromise between thermomechanical stability and overall diagnostics quality.

This paper presents a numerical methodology to analyse the coupled thermomechanical properties of an OTR screen on the basis of its different material properties and predict its diagnostics performance by means a preliminary study of the optical performance. The developed methodology represents a robust tool for machine designers to identify the most performing material and to understand its measurement reliability during long term operation (even considering the impossibility to test and validate the screen on facilities with comparable beam properties). For this reason, in our study two different materials are investigated: Aluminium (Al) and monocrystalline Silicon (Si). They were selected on the experimental evidence obtained in other high brightness quality machines. The goal is to illustrate how the developed methodology can be used to identify which of these two solutions may offer the best thermal, mechanical and optical performances considering the high charge beam of the GBS machine. The first part of the paper introduces the theoretical analysis used to preliminarily investigate the thermal behaviour of the OTR screen, while the second one uses the previous results to validate and to set up a Finite Element Analysis (FEA) to assess in detail the thermal behaviour of this diagnostic device, especially under a high number of consecutive thermal cycles due to the pulse succession. The FEA also explores the resulting mechanical behaviour of the OTR screens in terms of stress and strain distribution as well as the fatigue lifetime. Eventually, the last part concerns the optical behaviour in order to preliminary evaluate the consequences of thermal deformations on the optical resolution and to establish which is the most appropriate material between Al and Si to be used for the OTR screen in the GBS machine.

2. Theoretical analysis

An analytical approach was adopted to preliminarily study the thermal behaviour of the OTR screen in operation. This first step was essential to gather information about the maximum temperatures following one pulse impinging the OTR screen as well as a possible cumulative effect due to the pulse succession.

When a single particle interacts with matter, the energy deposition is proportional to the stopping power, material density and material thickness. Assuming an electron beam with a Gaussian "transverse distribution", the time evolution of the temperature on a target can be evaluated by solving the following equation [13]:

$$\frac{\partial T(x,y,t)}{\partial t} = \frac{1}{c_p \rho}\left\{ \frac{\partial E}{\partial z}\frac{Ne(t)}{2\pi\sigma_x\sigma_y}\exp\left(-\frac{x^2}{2\sigma_x^2}-\frac{y^2}{2\sigma_y^2}\right) + k\nabla^2 T(x,y,t) - \frac{2\epsilon\sigma_{sb}}{\Delta z}\left[T(x,y,t)^4 - T_0^4\right]\right\}. \quad (1)$$

The x and y are the coordinates of the beam interaction points on the OTR screen surface (z is the orthogonal axis on that surface, i.e. the

beam axis); $\partial E/\partial z$ is the electron stopping power, measured in eV/m and *Ne(t)* is the number of electrons in a pulse; (σ_x, σ_y) are the Root Mean Square (RMS) of the transverse beam size; Δz is the thickness of the screen; ρ is the density; c_p is the specific heat capacity; k is the thermal conductivity; ϵ is the emissivity of the material and σ_{sb} is the Stephan–Boltzmann constant. The first addendum of the Eq. (1) represents the temperature rise due to the interaction between the beam and a target, the second one is the cooling by conduction and the third one is the radiative cooling [14].

Since the OTR screen is in vacuum, there is no convection cooling. Furthermore, since the maximum temperature estimation of the OTR screen used in the GBS machine is few hundred kelvins, the radiative cooling can be considered negligible. It is worth noting that the temperature rise depends linearly on the bunch charge, and it is exponentially inversely with the beam size, while it is independent from the thickness of the screen (if the stopping power is constant along the beam axis). Besides, considering the GBS bunch separation of 16 ns, the cooling between the consecutive bunches of the same pulse can be neglected: only the cooling between bunch trains spaced 10 ms has been taken into account.

Considering the above assumptions, the solution of Eq. (1) in terms of ΔT is (1):

$$\Delta T(x,y,t) = \frac{\sigma_x}{\sqrt{2\alpha_d t+\sigma_x^2}}\frac{\sigma_y}{\sqrt{2\alpha_d t+\sigma_y^2}}\Delta T(0,0,0) \times \exp\left(-\frac{x^2}{2\left(2\alpha_d t+\sigma_x^2\right)}-\frac{y^2}{2\left(2\alpha_d t+\sigma_y^2\right)}\right), \quad (2)$$

$$\Delta T(0,0,0) = \frac{\partial E}{\partial z}\frac{Ne}{c_p\rho 2\pi\sigma_x\sigma_y}, \quad (3)$$

$$\alpha_d = \frac{k}{c_p\rho}. \quad (4)$$

The term α_d in the solution Eq. (2) is the thermal diffusivity of the target material, k the thermal conductivity, c_p the specific heat capacity and ρ the material density.

Fig. 2 illustrates the evolution in-time of temperature at the centre of the OTR surface (x = y = 0) where the beam hits the screen after one pulse (10 ms), considering the electron beam properties of the GBS machine (Table 1) and referring to both materials under test (Al and Si). The physical properties of the materials are described in Table 2. The first pulse causes a temperature rise of several tens of degrees, 350.6 K for the Al and 365.8 K for the Si, but still far from the melting point. Moreover, Fig. 2 shows that, even exponential behaviour, the temperature does not return exactly to the starting temperature at the end of the delivered impulse and before the next one starts (10 ms). In fact, at the end of one pulse, the temperature at the screen centre, in the interaction point, is still slightly higher, about 0.2 K, than the starting temperature of 295.15 K for both materials. This evidence shows that the maximum and the minimum temperature at the screen centre increase pulse by pulse, due to the energy deposition and accumulation. The different maximum temperature of the two materials is mainly due to their different specific heat capacity.

According to the above considerations, it was considered of interest to carry out a study – through a dedicated numerical analysis – to understand at what point thermal equilibrium will be reached after the energy deposit and accumulation. In fact, literature does not propose similar studies and theoretical approaches to evaluate the mechanical stress and deformations. Only some studies have been done using the Basquin's law [16], but this method is reliable only after a very large number of cycles. On the other hand, numerical simulations, that will be describe in the following sections, show that there are significant effects just after a low number of cycles. Moreover, another motivation is the validation of the theoretical analysis with a numerical one from FEA simulations. Therefore, in order to understand the significance of the temperature difference of 0.2 K from the starting point for both materials and to evaluate its spatial distribution, it has been decided to determine if the OTR screen temperature reaches an equilibrium state due to the deposited and dissipated heat, during the succession of impulses, by means FEA.

Table 1
Electron beam properties of the GBS machine used in the study.

Properties	GBS machine
Spot size along x-axis (rms), σ_x	47.5 μm
Spot size along y-axis (rms), σ_y	109 μm
Bunch charge	250 pC
Bunch pulse	32
Bunch spacing	16 ns
Pulse spacing (Repetition rate)	10 ms
Pulse length (rms), Δl	512 ns
Number of electron in a pulse, Ne	4.99×10^{10}
Electron stopping power (Al), $\partial E/\partial z$	8.65×10^{-11} J/m
Electron stopping power (Si), $\partial E/\partial z$	7.47×10^{-11} J/m
Peak of power density, Q_{max}	2.2×10^{14} W/m^3

Table 2
Materials properties of the OTR screen [15].

Properties	Aluminium (Al) AW – 6060 T6	Silicon (Si) Monocrystalline
Young's modulus, E	69 GPa	150 GPa
Poisson modulus e, ν	0.33	0.17
Ultimate tensile strength σ_R	190 MPa	124 MPa
Density, ρ	2700 kg/m^3	2330 kg/m^3
Coefficient of Thermal expansion,	23.0×10^{-6} K^{-1}	2.5×10^{-6} K^{-1}
Thermal conductibility, k	209.0 W/m/K	143.5 W/m/K
Specific heat capacity, c_p	890 J/kg/K	700 J/kg/K
Thermal diffusivity, α_d	8.7 m^2/s	8.8 m^2/s

3. Finite element simulations

The finite element simulations allowed the coupling of the thermal with the structural analysis and the calculation of the deformation-stress field following the temperature cycles in the OTR screen. Moreover, they allowed the prediction of the thermomechanical behaviour of the OTR screen for a very large number of consecutive cycles, one for each beam pulse, which is a fundamental condition for the applicability of the fatigue theory. The simulations were performed with ANSYS®Mechanical APDL code.

3.1. Thermal analysis

The OTR screen (30 × 30 × 1 mm) was modelled with a structured 3D mesh using ANSYS SOLID70 elements [17] and the mesh was refined in the beam impact area, hereafter "hotspot", in the centre of the OTR screen, where heat is generated (Fig. 3).

The power density Q, associated to the internal heat generation due to the interaction between the electron beam and the OTR screen material, was implemented and modelled in the ANSYS®environment through an APDL script [18]. Spatially, the power density Q has been modelled as a Gaussian distribution along the OTR screen surface with the peak in the screen centre, as reported in the subsequent Eq. (5); while, temporally, it has represented with a pulsed behaviour with a high (100 Hz) repetition rate: active during the pulse interaction (512 ns) and inactive until the impact of the successive pulse (10 ms). The APDL script allowed modelling all these spatial and temporal distributions of the surface power density Q as following:

$$Q(x,y) = Q_{max}\cdot e^{-\frac{1}{2}\cdot\left[\left(\frac{x}{\sigma_x}\right)^2+\left(\frac{y}{\sigma_y}\right)^2\right]}, \quad (5)$$

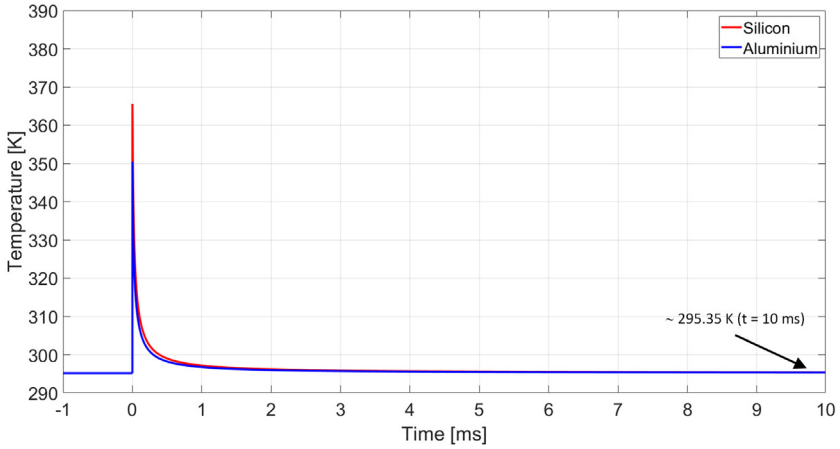

Fig. 2. Temperature evolution at the centre of the target due to the conduction cooling after the screen heating (10 ms time span, single pulse), according to Eq. (2), for GBS machine (Table 1). The plot compares Silicon (red line) and Aluminium (blue line) targets.

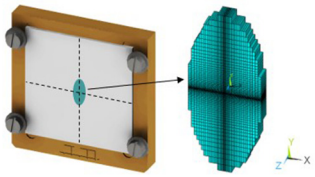

Fig. 3. OTR screen geometry and 3D mesh of the "hotspot" zone. The finite element model has been developed by means a structured and a progressive mesh refinement at the centre. The target discretization is based on SOLID70 ANSYS elements.

where

$$Q_{max} = \frac{\frac{\partial E}{\partial z} \cdot Ne}{\Delta l \cdot (2\pi\sigma_x\sigma_y)}. \quad (6)$$

Here, as well as for the Eq. (1), $\partial E/\partial z$ is the electron stopping power, measured in eV/m.

The script associates to each mesh element in the "hotspot" zone (where the mesh is finer) an internal heat generation equal to the power density calculated in the mesh element centroid. This discretization introduces a small inaccuracy in modelling of the power density Q. Obviously, the finer is the mesh in the hotspot, the more accurate is the modelling. For this reason, in order to evaluate the best mesh size for computational resources and solution results, a preliminary mesh sensitivity analysis has been done (Fig. 4). The plot shows the maximum temperature reached as a function of the minimum mesh size of the hotspot elements and the ANSYS® applied power density for both materials. The optimal mesh size was obtained for 0.3 μm.

Moreover, the comparison, reported in Fig. 5, confirms the accuracy of the APDL script power density modelling showing a difference of only ~0.5% respect to the analytical power density. This implies that even a temperature variation calculated in the order of tenths of a degree is reliable and realistic with this model.

Regarding the boundary conditions of the thermal transient analysis, the initial temperature of the OTR screen was considered equal to the GBS machine room temperature (295.15 K), as for the support frame and screws (Fig. 3). The properties of the two materials under test, Al and Si, were the same of the theoretical analysis reported in Table 2. Furthermore, considering the scenario along the LINAC of the GBS machine (Table 1), the geometry of the spot size was assumed as a highly focused electron beam with an elliptical shape.

The results of the thermal simulations are reported in the following figures. Fig. 6 shows the peak temperature distribution in the "hotspot" after the impact of a single beam pulse (512 ns). The maximum temperature for the Al screen is 349.7 K, while for the Si screen is 364.5 K. For both materials, the heated area represents a limited portion of the OTR screen determining a high temperature spatial gradient. Si shows a higher temperature increase than Al and this can be considered as an expected result considering its lower density and lower specific heat capacity. The difference in the temperature increase respect to the theoretical analysis is 0.9 K for Al (0.3%) and 1.3 K for Si (0.4%).

Table 3
Temperature decay after the first pulse: Al and Si screen.

Decay level (wrt max)	Al		Si	
	Temperature	Decay time	Temperature	Time
90%	344.2 K	0.002 ms	357.5 K	0.002 ms
10%	300.8 K	0.272 ms	302.3 K	0.272 ms
Difference	**43.4 K**	**0.271 ms**	**55.2 K**	**0.271 ms**

Instead, Fig. 7 shows the time evolution after the screen heating for 1 ms. The figure refers to the centre of the impact area of the beam on the OTR screen ($x = y = 0$). It reproduces the same results obtained in the previous section by using the analytical model, including a small increase of starting temperature for the second pulse.

Eventually, Table 3 reports the time necessary to decay to the 90% and the 10% of the temperature increase after the first pulse for, respectively, the Al and the Si screens. The cooling transient is very quick, and it decays following an exponential trend. This is due to the initial high temperature gradient that determines a very efficient heat discharge around the "hotspot" area through thermal conduction in the first fractions of ms. The table shows that the temperature decays from the 90% to the 10% of the peak in less than 3% of the pulse spacing. After that, the temperature slows down its decay and follows a small temperature decrease of ~0.05 K/ms. The residual temperature after one pulse is minimal as noted. Therefore, the results of the simulations confirm the analyses of the previous theoretical analysis (Fig. 2)

Simulating 500 consecutive thermal cycles (corresponding to 5 s of machine operation), the thermal simulations bring evidence that there are no important cumulative effects due to the observed residual temperature, for neither of the investigated materials. There is not any critical increase neither for the minimum nor the maximum temperatures that reach stable values in a very short time, after few oscillations. This temperature oscillation reaches the steady-state condition after 2.01 s and 1.92 s for, respectively, the Al and the Si screen as reported in Table 4.

Concluding, the results confirms that the thermal oscillation of the OTR screen during the machine operation is compatible with the material properties under test. However, although the maximum temperatures do not reach the melting point of the selected materials, the stress and strain generated on the OTR screen surface deserves further

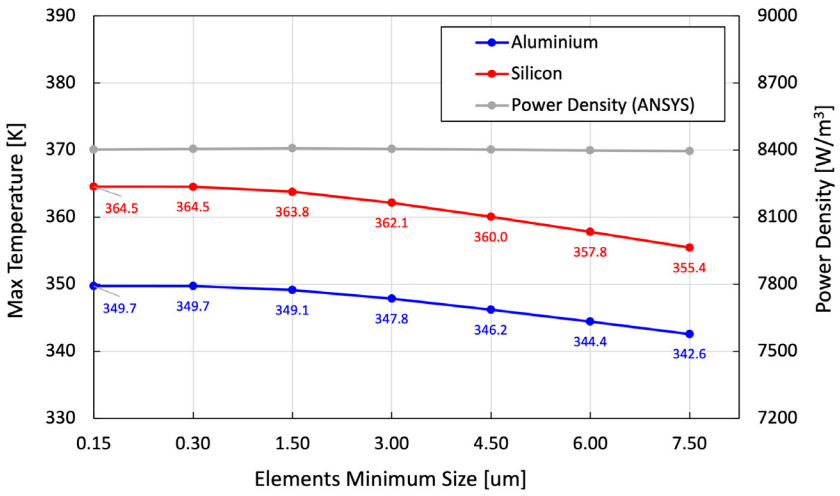

Fig. 4. Preliminary finite element mesh sensitivity analysis: the plot shows the maximum temperature reached as a function of the minimum mesh size of the hotspot elements and the applied power density for both materials.

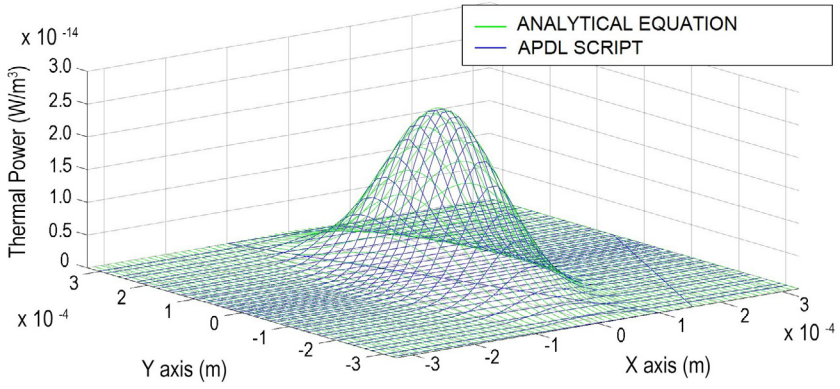

Fig. 5. Comparison between the analytical power density Q and the one that the APDL script models (x–z plane).

Table 4
Steady-state thermal cycle. Oscillation between maximum and minimum constant temperature value VS the maximum and minimum temperature after the first impact (10 ms).

Material	T_{max}	T_{min}	Time
Aluminium (Al)	349.7 K	295.3 K	10 ms
	350.5 K	296.1 K	2.01 s
Silicon (Si)	364.5 K	295.4 K	10 ms
	365.6 K	296.3 K	1.92 s

Table 5
Equivalent Von Mises stress and displacement results.

Equivalent stress and displacement	Al screen	Si screen
Maximum Von Mises stress (σ_{VMmax})	54 MPa	12 MPa
Minimum Von Mises stress (σ_{VMmin})	0.13 MPa	0.04 MPa
Maximum displacement	147 nm	16 nm

investigations in order to evaluate their fatigue lifetime and optical performance.

3.2. Structural analysis

The structural analysis modelled the OTR screen with the same mesh geometry of the thermal one, with the only difference of using the ANSYS SOLID185 elements [17]. The static structural linear analysis of the OTR screen used as input the results of the thermal one: the temperatures calculated on the "hotspot" zone at the maximum peak temperature for the first thermal cycle (512 ns) (Fig. 7), were transferred to each new mesh node to evaluate stress and strain.

The results of the structural simulations are reported in the following figures. Fig. 8 shows the distribution of the equivalent Von Mises (VM) stress [19], and as predictable, the maximum stress values for both materials are located in the OTR screen centre, where the screen surface reaches maximum temperature and deformation. On the other hand, there are no stress where the temperature field remain at the initial temperature of 295.15 K. Table 5 reports the maximum and the minimum values of VM stress for both materials as well as the associated maximum displacement vector, representing the module of the vector composed by the individual displacement along x, y and z, as reported in Eq. (7):

$$|\vec{u}| = \sqrt{u_x^2 + u_y^2 + u_z^2}. \tag{7}$$

Moreover, Fig. 9 depicts the displacement vector contour plot for both materials: the displacements along x, y is almost comparable.

Considering the results in terms of equivalent VM stress and maximum displacement and despite the higher increase of temperature, the Si screen achieved the better mechanical performance. It is worth noting that the maximum displacement in Si screen is about one order of magnitude lower than the Al screen, becoming the candidate for the material offering the best optical performances as illustrated in the next section.

A rough estimation of the impact of the deformation to the beam profile can be done using simple geometric optics. Indeed, the deformation introduce an angular deviation in the optical beam that may

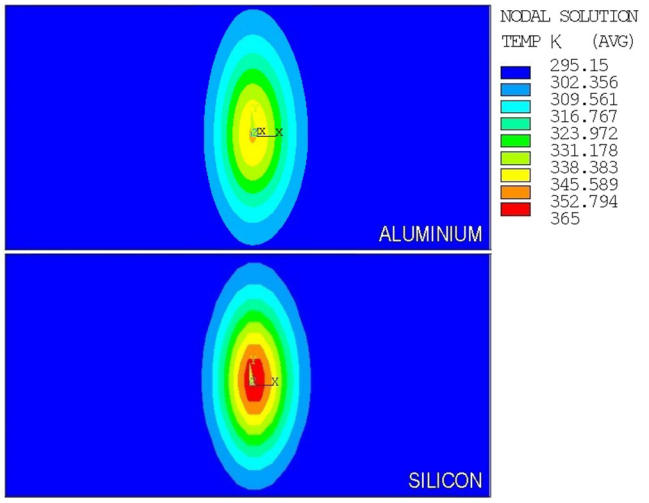

Fig. 6. Temperature field in the "hotspot" – for both materials – at the maximum peak temperature for the first pulse (512 ns).

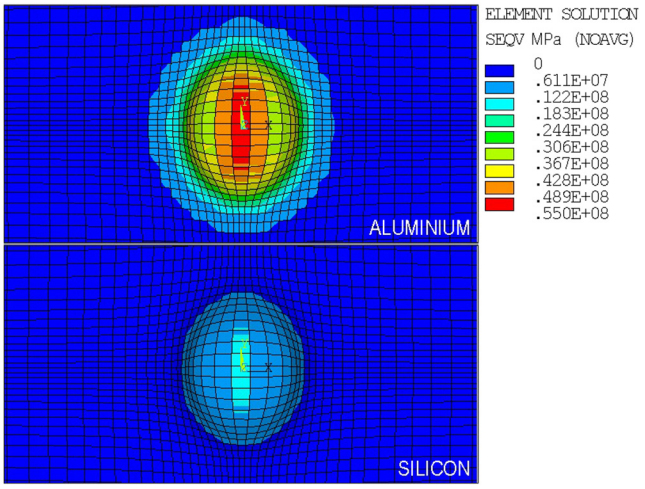

Fig. 8. Equivalent Von Mises stress on the "hotspot" – for both materials – at the maximum peak temperature for the first pulse (512 ns).

impact the beam spot-size measurements, both in terms of number of photons collected by the optic system and in the transverse size measurements. For instance, considering a transverse beam size of $3^*\sigma$ (i.e., 3*47 um = 141 μm in horizontal and 3*107 = 327 μm in the vertical plane), the angular deviation is ~0.1 mrad horizontal and ~0.04 mrad in vertical plane considering the Al displacement. These values are not negligible, and they may affect the optical performance: in Section 4, a preliminary study performed with the optical simulation software will be presented.

Eventually, the maximum stress in both materials is below their ultimate tensile strength without any risks of static fracture failure. However, the cyclic nature of the mechanical loading that the OTR screen has to withstand may result in a fatigue damage. Next paragraph illustrates how the fatigue theory was integrated in the developed methodology.

3.3. Fatigue life evaluation

The evaluation of the OTR screen lifetime uses as input the stress calculated through the structural linear analysis (Table 5). Generally, the main factors contributing to the fatigue damage are the number of load cycles, the stress range and the concentration of local stress. The last one was neglected for the OTR screens considering their square geometry. In spite of the rapid phenomena and the narrow timescale, the structural analysis has shown non-negligible deformations for the OTR screen. They may have an impact on the OTR optical performances as well as they may bring to a screen fatigue failure considering the high frequency cyclic nature of the following stress. In fact, in some cases, when the fatigue process is time-dependent, then it also becomes frequency-dependent particularly when high temperatures are encountered [16] and the cyclic rates become more important. For this reason, an evaluation of the fatigue lifetime of the OTR screens has been performed

The equivalent Von Mises stress has been used to estimate the alternating (σ_a) and the mean (σ_m) stress magnitude:

$$\sigma_a = \frac{\sigma_{VMmax} - \sigma_{VMmin}}{2}; \sigma_m = \frac{\sigma_{VMmax} + \sigma_{VMmin}}{2}. \quad (8)$$

To estimate the effects on the OTR screen material of the alternating and mean stress, it has been applied the well-known Goodman

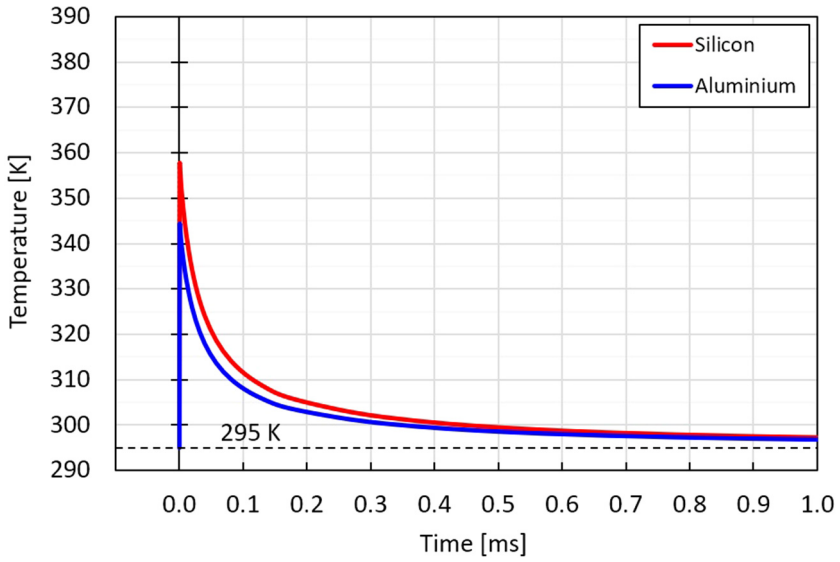

Fig. 7. Temperature evolution of the screen during 1 ms after the beam impact (FEA simulations). The figure refers to the centre of the impact area of the beam on the OTR screen ($x = y = 0$). The plot compares Silicon (red line) and Aluminium (blue line) targets.

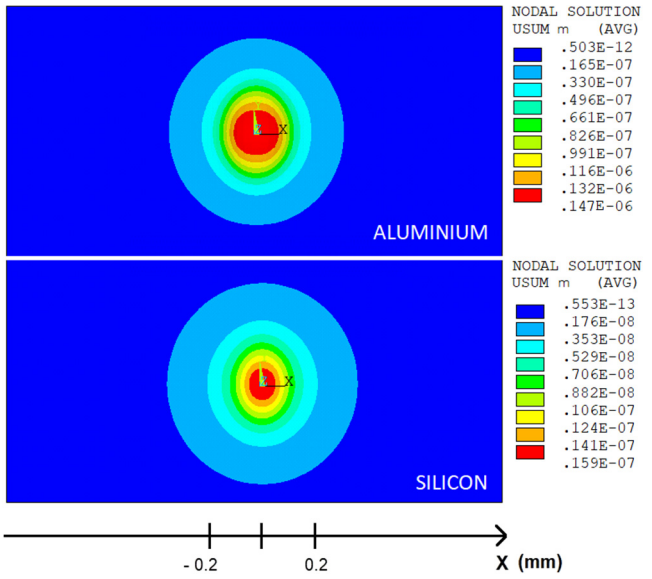

Fig. 9. Profiles of the displacement vector sum u [m] – for the candidate materials – reached at the maximum peak temperature for the first pulse (512 ns).

theory [16], represented by the Eq. (8), in which σ_R is the material ultimate tensile strength and σ_N the Goodman alternating stress level:

$$\frac{\sigma_a}{\sigma_N} + \frac{\sigma_m}{\sigma_R} = 1. \tag{9}$$

The Goodman relation describes the decreasing of the fatigue life with an increase of mean stress level for a given level of alternating stress. Once evaluated the Goodman alternate stress level (σ_N), the number of cycles to failure (N) were calculated by means the S–N Wohler for each material [20,21]. Consequently, the fatigue material damage has been determined with the Miner theory, represented by the Eq. (9):

$$D = \sum_{i=1}^{n} \frac{n_i}{N_i}. \tag{10}$$

According to Miner approach, the fatigue damage is given by the sum of the relative damages at each level of load which in this case corresponds to the set of beam properties for each machine operation mode. The cumulative damage is proportional to the ratio between the number of cycles that have taken place (n_i) and the number of cycles (N_i) which causes the component failure for that stress level [21].

Table 6
Fatigue life evaluation results.

Fatigue lifetime parameter	Aluminium (Al)	Silicon (Si)
Goodman alternating stress (σ_N)	30 MPa	8 MPa
Number of cycles to failure (N)	609700	∞
Cumulative fatigue damage after one operating hour (D)	0.59	0.00

Table 7
Sensitivity analysis for different number of bunches: Al screen.

Number of bunches (n_b)	Maximum temperature (T_{max})	Goodman alternating stress (σ_N)	Number of cycles to failure (N)
32	350.5 K	30 MPa	609700
16	320.2 K	14 MPa	∞
8	307.7 K	7 MPa	∞
4	301.1 K	3 MPa	∞

The failure occurs if the total damage (D) ≥ 1. The limitation of this approach is that the Eq. (9) does not consider the real sequence of mechanical stresses. However, this limitation does not affect the damage calculation for the considered case study since only the operation mode corresponding to the beam properties in Table 1 is considered, therefore the load cycles are equal (i = 1).

Using the Von Mises stress from Table 5 and Eq. (7), and the values for the ultimate tensile strength σ_R [15], the Goodman alternate stress for the Al and Si screens are inferred to be 30 MPa and 8 MPa. Table 6 reports the results of the lifetime evaluation, considering the number of cycles to failure N [20,21] and one operating hour (360000 thermo-mechanical cycles). In this case, the OTR Al screen reaches a cumulative fatigue damage of 0.59, while the Si screen has not any fatigue limit. Therefore, the methodology predicts the failure of the OTR Al screens in less than two hours for the high beam performance, while the same methodology predicts that the OTR Si screens will not suffer of fatigue fracture.

On the other hand, changing the characteristic of the electron beam, for example decreasing the number of bunches (n_b) for pulse, the fatigue life for the Al screen increases up to no fatigue limit as the Si screen for nominal n_b. As a matter of fact, for lower n_b, the reached peak temperatures (Fig. 10) as well as the mechanical stress are lower: consequently, the maximum number of loading cycle before the fatigue failure is inversely proportional to the number of beam bunches (Table 7). This result can be used to avoid progressive damage to the screen.

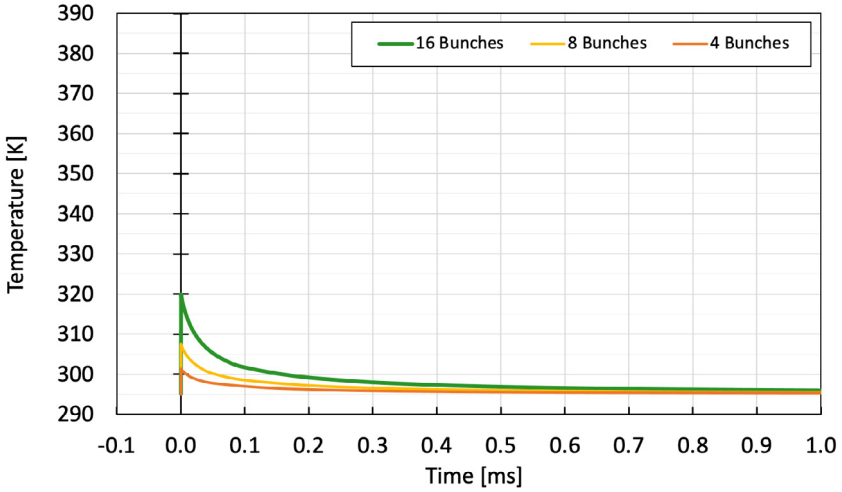

Fig. 10. Temperature evolution after the screen heating (1 ms) changing the number of bunches (16, 8 and 4) for the Al screen. The figures refer to the centre of the impact area of the beam on the OTR screen ($x = y = 0$).

Fig. 11. Profile of the unperturbed and deformed OTR screen. Arrows define the sag displacement direction [10] as implemented in ZEMAX.

4. Preliminary studies on the optical performance

A distortion of the OTR screen surface close to the electron beam hotspot may generate a loss of image resolution [18]. Therefore, considering the intrinsic functionality of the OTR, the evaluation of the surface strain is crucial to confirm the predicted optical performance. The prediction of the optical performances is typically done with commercially available optical design software such as ZEMAX® [22]. This software allows to represent surface errors and displacements by means of polynomial surface definition, surface interferogram files or uniform array of data. The surface errors are defined by means of surface normal or sag displacement (Fig. 13): the sag displacement is defined as the distance from the vertex tangent plane to the optical surface. It is important to note that, following the convention used for example in ZEMAX®software, the sag value is measured from the ideal to the deformed surface as shown in Fig. 11.

The physical problem of an OTR screen can be approximated to the reflection of a deformed mirror: the photons reflected are then collected by an optical system to perform the imaging of the source as it is shown in the scheme of Fig. 1. This approximation was made because ZEMAX® does not allow to implement the deformation directly in the source of radiation. Due to the fact that OTR is emitted with an angle inversely proportional to the beam energy, this approximation holds only with limited choice of beam energy and optical geometry (distance between lenses). In the case presented in this paper, this results in a conservative approach. For this reason, the propagation of a laser beam through a mirror has been simulated: the beam has the same spot size as the electron beam under study (Table 1), the mirror has the same 45° tilt as in Fig. 1 and the same displacement as the one created by the beam on the Al and on the Si target by finite element simulations (maximum displacement of 147 nm and 16 nm respectively, as can be seen in Table 5).

The optical analysis with ZEMAX® show how the deformation, evaluated with finite element analysis, causes a small translation of the centroids of the beam (below 1.4 μm for the Si case and below 10 μm

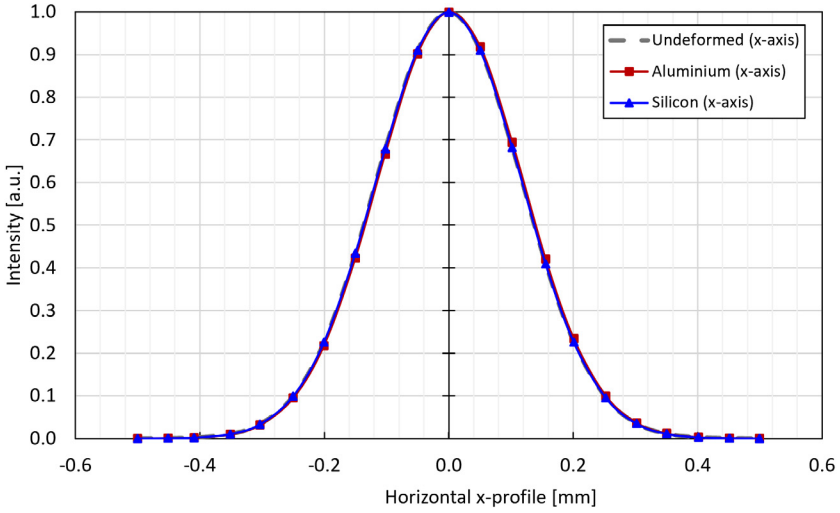

Fig. 12. Light beam profile at the CCD camera location for the screen without deformation and for the Al and the Si deformed screen (x-axis).

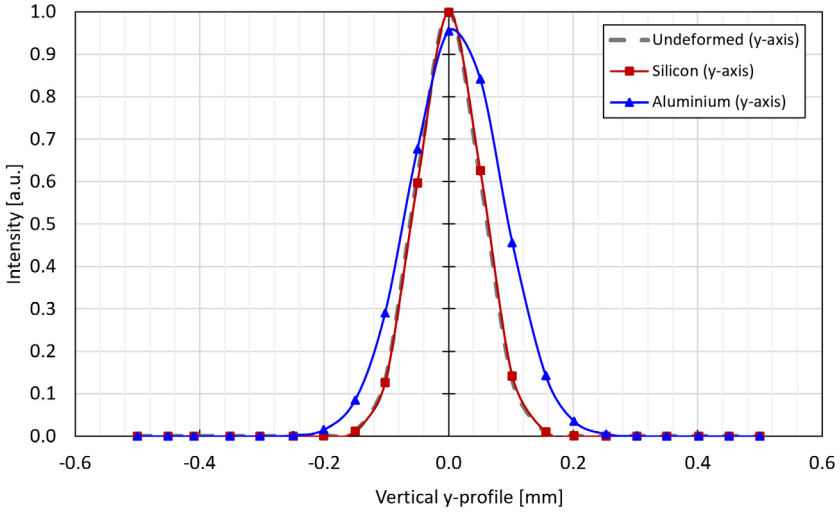

Fig. 13. Light beam profile at the CCD camera location for the screen without deformation and for the Al and the Si deformed screen (y-axis).

for the Al case) and a loss of the collected photons which is negligible for the Si case (0.4%) while it goes to 30% for the Al case. During the analysis, a bigger issue was related to the Gaussian reconstruction of the beam shape in the case of the Al: the measurement error is negligible for the x profile evaluation ($\sigma = 47.5$ μm) while is 44% in the y plane ($\sigma = 109\mu$m), as can be seen in Figs. 12 and 13. Here, the σ values are intended as the expected ones.

Such error dependence on the spot size has been confirmed also by other simulations for different beam size: for instance, a 27 μm symmetric beam get deformed by a factor less than 1%. This is true if the 27 μm beam has the same charge density, hence the same energy deposition into the screen. For a different charge density, instead, a new deformation simulation has to be done. Also, the centroids and the amplitude are less affected by the displacement; the effect is more significant on the y plane, where the deformation of the screen is larger due to the asymmetry of the beam that cause the deformation. The reason is related to the area of displacement where the beam is reflected: a bigger beam is reflected by a larger area of the deformed mirror. Indeed, the larger beam "sees" a bigger portion of the displacement. Further studies are possible like, for instance, evaluating different beam size and charge density or the effect of a tilt in the screen. These analyses are indeed foreseen in the future.

These results show that the optical properties of the Si screen do not change significantly even after the thermal deformation. For this reason, we have chosen Si as OTR screen material. The Si target comes from the same production line of the Si disks used for the electronic devices, whose main characteristic is the flatness of the surface. The performances of the Al screens, for such high charge densities, are instead seems to be heavily compromised.

5. Conclusion

This paper presents a finite element methodology to assess the thermomechanical and optical performances of the OTR screens for beam diagnostics in high brightness/high charge electron LINAC such as the GBS facility. The study consists in carrying out the thermal and structural transient analysis accounting for the interactions of the bunches with the OTR screen during the machine operation i.e., implementing the Gaussian spatial distribution of the particles in the bunch through a dedicated ANSYS®ADPL script. The output of the structural finite element analysis is used for a fatigue and optical study: the mechanical stress is used to determine the lifetime of the screen according to the classic fatigue theory, whereas the deformations are used with ZEMAX®software to perform a preliminary study the optical quality of the diagnostic system, since the thermally inducted deformations affect surface flatness.

Following this methodology, we compared the performances of two different materials: Al and monocrystalline Si. The analysis confirmed the choice of the Si for the OTR screens in the GBS facility as initially predicted by a preliminary theoretical analysis [14,23]. During the machine operation, the Si screen reaches higher temperature in the thermal oscillations than the Al one. Nevertheless, for the nominal beam conditions, its better mechanical properties determine a better behaviour in terms of stress and deformation reflecting in an infinite number of cycles to failure (while the Al is limited to only two hours of operation) and in superior optical performances. Furthermore, the described methodology can be applied to several and different cases of study involving an interaction between electron beams and materials, since it is possible to change each single problem parameter such as the OTR screen geometry and material, and the beam properties including the spatial Gaussian distribution. In this way, it is possible to simulate different operation conditions for the same GBS, but also for other machines using OTR screens for the beam diagnostics, to identify the solution for the OTR design fitting the machine requirements and for industrial application with highly focused radiation hitting material for different purposes [24].

Declaration of competing interest

The authors declare that they have no known competing financial interests or personal relationships that could have appeared to influence the work reported in this paper.

References

[1] A. Bacci, et al., Electron LINAC design to drive bright Compton backscattering gamma-ray sources, J. Appl. Phys. 113 (19) (2013).
[2] D. Alesini, et al., Status of the SPARC project, Nucl. Instrum. Methods Phys. Res. A, 528 (1–2), 586-590.
[3] Antici, et al., Laser-driven electron beamlines generated by coupling laser-plasma sources with conventional transport systems, J. Appl. Phys. 112 (2012) 044902.
[4] A.R. Rossi, et al., The External-Injection experiment at the SPARC_LAB facility, Nucl. Instrum. Methods A 740 (2014) 60–66.
[5] V.L. Ginzburg, I.M. Frank, Radiation of a uniformly moving electron due to its transition from one medium into another, Zh. Eksp. Teor. Fiz. 9 (1945) 353–362.
[6] M. Marongiu, et al., Energy measurements by means of transition radiation in novel linacs, Nucl. Instrum. Methods Phys. Res. Sect. A (2018).
[7] L. Sukhhikh, Simulation of transition radiation-based beam imaging from tilted targets, PRAB 20 (2017) 032802.
[8] F. Cioeta, et al., Thermal Simulation for Optical Transition radiation screen for GBS-GBS Compton gamma source. Proceedings of IBIC2016, Barcelona, Spain.
[9] Jackson, Classical Electrodynamics – Wiley, 478-506.
[10] Marc. Ross, et al., A very high-resolution optical transition radiation beam profile monitor, in: Proceedings of BIW02, Upton, New York U.S.A.
[11] E. Chiadroni, et al., The SPARC linear accelerator-based terahertz source, Appl. Phys. Lett. 102 (9) (2013) 141117, 4475.
[12] C. Vaccarezza, et al., The SPARC_LAB Thomson source, Nucl. Instrum. Methods Phys. Res. A 829 (1) (2016) 237–242.
[13] E. Bravin, et al., Otr studies for the high charge CTF3 beam, in: Particle Accelerator Conference, 2003. PAC 2003. Proceedings of the, vol. 4, IEEE, 2003, pp. 2464–2466.
[14] M. Marongiu, et al., Thermal behaviour of the optical transition radiation screens for the GBS-gbs compton Gamma source, Nucl. Instrum. Methods Phys. Res. Sect. A 865 (2017) 47–50.
[15] Material parameters: http://www.matweb.com/.
[16] J.E. Shigley, et al., Mechanical Engineering Design, Mc Graw Hill, 2014.
[17] ANSYS® Inc., Ansys® mechanical APDL theory reference, release 15.0, 2013.
[18] F. Cioeta, et al., Multi-purpose ansys APDL script developed for analysis of matter-radiation interaction, in: Enginsoft Newsletter, Spring, 2019, pp. 27–31.
[19] Continuum mechanics: http://www.continuummechanics.org/vonmisesstress.html.
[20] G.T. Yahr, Fatigue Design Curves for 6061-T6 Aluminium, Engineering Technology Division, Oak Ridge National Laboratory, Oak Ridge, Tennessee, 37831-8051.
[21] M.J. Kirkham, Advances in Ultra-High Cycle Fatigue. University of Tennessee, Knoxville.
[22] Zemax Optic Studios: https://www.zemax.com/products/opticstudio.
[23] M. Marongiu, et al., Design issues for the optical transition radiation screens for the GBS Compton Gamma Source. Proceedings of IPAC2016, Busan, Korea.
[24] F. Cioeta, et al., Simulation of thermo-mechanical effects produced by a highly focused radiation applied on a material: developing of a multi- purpose APDL script for the physical characterization. CAE Conference, 8-9 2018 Vicenza- Italy.